Materials & Design 248 (2024) 113524

Contents lists available at ScienceDirect

Materials & Design

journal homepage: www.elsevier.com/locate/matdes

High-temperature mechanical behaviour of Al-10Ce alloy with Sc, Zr, Si, and Mg alloying elements

Shishir Keerti [a,*], Pavel Shurkin [a], Qing Cai [a], Hari Babu Nadendla [a], Animesh Mandal [b]

[a] BCAST, Brunel University of London, Kingston Lane, Uxbridge, Middlesex UB8 3PH, United Kingdom
[b] School of Minerals, Metallurgical and Materials Engineering, Indian Institute of Technology Bhubaneswar, 752050 Odisha, India

ARTICLE INFO

Keywords:
Al-Ce alloys
Elevated temperature mechanical properties
Thermal stability
High pressure die casting

ABSTRACT

The influence of Sc, Zr, Mg, and Si addition to Al-10Ce hypereutectic alloy on the formation of intermetallics and mechanical properties have been investigated in as-cast condition and after heat treatment. The incorporation of Sc and Zr facilitated the formation of primary Al_3 (Sc, Zr) intermetallics, which effectively refined the α-Al grains due to heterogeneous nucleation. Si addition resulted in the formation of the Al_2CeSi_2 phase. Aging at 300 °C led to the formation of nanoscale Al_3(Sc, Zr) precipitates with an average diameter of 3 nm. The hardness of the alloy significantly increased and remained unaffected even after ageing for 100 h which suggests the thermal stability of the Al-Ce alloy containing these precipitates. As a result of thermal stability, Al-10Ce-(Sc, Zr) is observed to exhibit higher yield strength at 300 °C than a range of Al-Cu, Al-Si alloy systems.

1. Introduction

The earliest studies of high-strength, thermally stable aluminium alloys date back to 1950 [1,2]. Rare earth elements, particularly cerium (Ce), have shown great potential in enhancing high-temperature properties, mechanical strength, and microstructural modification of aluminium alloys. Due to its abundance and cost-effectiveness, Ce in new Al-Ce-based alloys not only reduces material costs but also imparts beneficial properties, such as improved castability, and high-temperature strength [3–5]. Ce exhibits negligible solubility (0.05 wt % Ce at 640 °C [6]) and diffusivity of Ce ($D_{Ce/Al} = 4.65 \times 10^{-19}$ m^2/s at 400 °C [7]) in (Al) matrix and forms a thermally stable $Al_{11}Ce_3$ intermetallic solidified through a eutectic reaction at 645 °C [8].

Liu et al. [9] demonstrated the superior thermal stability of Al-12.5Ce, showing negligible hardness change after 12 weeks of isothermal aging at 400 °C. Similarly, Al-9Ce exhibited no hardness change after 720 h (h) at 350 °C [10]. Although the $Al_{11}Ce_3$ intermetallic phase is hard (350 HV), its strength contribution is limited due to its incoherent interface with Al [11]. The room temperature yield strength (YS) of Al-Ce alloys ranges from 30 MPa (Al-6Ce) to 68 MPa (Al-16Ce) [12], with lower strength degradation at elevated temperatures compared to conventional Al and Mg alloys. For example, at 300 °C, Al-9Ce [10] shows a 25 % YS reduction (60 MPa to 45 MPa), while Al-10Si [13] alloy exhibits 50 % reductions, from 110 MPa to 55 MPa.

Alloying with elements like Mg, Y, Sc, Si, and Zr enhances the mechanical properties of Al-Ce alloys while preserving their thermal stability. For instance, David Weiss [14] found that Al-8Ce-10 Mg alloy exhibited significantly higher mechanical strength at elevated temperatures compared to conventional piston alloys. Similarly, Wang et al. [15] demonstrated that Al-8Ce-3Y alloy, cast using high-pressure die casting (HPDC), significantly outperformed conventional piston alloys at 300 °C. Sc and Zr are suitable alloying elements for producing high-temperature heat-treatable alloys, Sc and Zr exhibit limited diffusivity ($D_{Sc/Al} = 2 \times 10^{-17}$ m^2/s [16]) and Zr ($D_{Zr/Al} = 1.2 \times 10^{-20}$ m^2/s [17]) in Al matrix, and forms Al_3Sc and Al_3Zr precipitates respectively. Addition of Sc has proven to elevate the strength of Al alloy by optimum ageing. For example, the hardness of Al-0.18Sc alloy was increased from 20 to 80 HV by ageing at 300 °C [18]. In another study by Seidman et al. [19], it was demonstrated that the micro alloying with Sc(<3 wt%) improved the creep resistance up to 300 °C. Although lean alloying with Sc provides good strengthening, it does not sustain the properties at temperatures higher than ~300 °C for long operating hours due to coarsening of Al_3Sc. To overcome this, Sc is commonly mixed with Zr while designing an alloy. Since the diffusivity of Zr in Al is low, the precipitates it forms are more resistant to coarsening than the Al_3Sc phase. In the Al-Sc-Zr system, the Al_3Sc precipitates form early during the ageing and act as the nucleation sites for Zr atoms, forming Al_3(Sc, Zr) precipitate with a core rich in Sc and an outer shell rich in Zr which

* Corresponding author.
E-mail address: Shishir.Keerti2@brunel.ac.uk (S. Keerti).

https://doi.org/10.1016/j.matdes.2024.113524
Received 21 October 2024; Received in revised form 27 November 2024; Accepted 3 December 2024
Available online 4 December 2024

provides resistance to coarsening [20,21]. Although the effect of Sc and Zr on Al alloys is well discussed in the literature, no significant study is available to evaluate the precipitation behaviour of Sc and Zr in Al-Ce alloys, especially its effect on high temperature performance of components manufactured by HPDC. L.Wang et al. [22] studied the effect of micro alloying of Al-5Ce with Sc(0.2 wt%) and Zr(0.2 wt%). The grain refinement behaviour of Zr and Sc on primary Al was significant along with the refinement of $Al_{11}Ce_3$ phase. The morphology of eutectic was modified from lamellae to thin rods with addition of Zr and this modification impacted the elongation, increasing from 17.5 % to 23 %. Same trend was followed by YS which was155MPa for Al-5Ce −0.2Sc-0.2Zr as compared to 49 MPa of Al-5Ce base alloy, after heat treatment. Similarly, Yi et al. [23] reported the influence of 0.4 wt% Sc addition on the creep behaviour of Al-12Ce alloy. The creep threshold stress at 300 °C was reported to increase from 12 MPa in Al-12Ce alloy to ~ 50 MPa in Al-12Ce-0.4Sc alloy. Mohammed et al. [10] studied the ambient and high temperature tensile behaviour of Al-9Ce, Al–9Ce–0.12Sc–0.02Zr, Al–9Ce–0.24Sc–0.04Zr and Al–9Ce–0.36Sc–0.06Zr alloys. Al–9Ce–0.36Sc–0.06Zr alloy showed the highest YS at both ambient (~185 MPa) temperature and at 300 °C (95 MPa). The enhancement in mechanical properties in these alloys was attributed to nanoscale Al_3(Sc, Zr) precipitates formed after aging.

Elements like Mg and Si are known to provide strengthening in Al alloys through effective solid solution and precipitation strengthening depending on the type of heat-treatment method. In Al-Ce alloys, Mg and Si have been reported to provide effective strengthening at room temperature. Sims et al. [24] reported the room temperature yield strength for Al-12Ce, Al-12Ce-0.4 Mg and Al-12Ce-4Si-0.4 Mg alloys as 57 MPa, 75 MPa and 78 MPa, respectively. After T6 heat treatment, an elevation in YS was observed in Al-12Ce-4Si-0.4 Mg alloys with reported YS being 128 MPa. Similarly, Hu et al. [25] studied the room temperature tensile behaviour of Al-8Ce-*y*Mg ($y = 0$, 0.10, 0.25, 0.50, 0.75 wt %) alloys prepared through HPDC. Due to solid solution strengthening by Mg atoms, the YS was observed to be increase from 92 MPa in base alloy to 115 MPa in case of Al-8Ce-0.75wt.%Mg.

The present study investigates the effect of Sc, Zr, Mg and Si on the thermal stability of the alloy and aims to expand the structural application of Al-Ce alloys at elevated temperatures by proposing a new Al-Ce-Sc-Zr-Mg-Si alloy which properties would benefit from fine microstructure provided by HPDC casting. For this purpose, the microstructure, thermal stability, room and elevated temperature tensile behaviour of hypoeutectic Al-10Ce alloy have been systematically studied. The leveraging phase composition and hardening mechanisms have been discussed.

2. Materials and methods

2.1. Alloy preparation

Model Al-10Ce alloys containing variable concentrations of Sc, Zr, Si and Mg were produced by adding appropriate amounts of Al-30wt.%Ce, Al-2wt.%Sc, Al-10wt.%Zr, Al-20 wt% Si and Al-10wt.%Mg master alloys to 99.99 % pure aluminium melt. The melt was prepared in a graphite-clay crucible in an electric furnace at a temperature of 780 °C. Part of the melt was gravity-cast into a preheated book mould with a cavity of 180mm × 170mm × 20mm, at a pouring temperature of 750 °C. Part of the melt was fed into a HPDC chamber to produce round tensile test bars. The alloy compositions were verified by optical emission spectrometer and listed in Table 1.

A Frech 4500 kN cold chamber HPDC machine was used to cast eight ASTM B557 standard round tensile test bars with a gauge dimension of ϕ6.35 mm × 50 mm in each shot. The dies were preheated by the means of hot oil at a temperature of 250 °C and the shot sleeve was preheated at 180 °C. During each shot, the mass of melt was fixed to ~800 g and the pouring temperature of the melt on the ladle was measured to be 720 °C before feeding into the shot sleeve. For all castings, the liquid metal injection speed (~2.3 m/s) and speed at the gate (~62 m/s) were fixed.

Table 1
Chemical compositions of all experimental alloys.

Nomenclature	Composition (wt.%)						
	Al	Ce	Sc	Zr	Si	Mg	Fe
Alloy 1	Bal.	10.2	0	0	0	0	<0.01
Alloy 2	Bal.	9.8	0	0.18	0	0	<0.01
Alloy 3	Bal.	9.3	0.22	0.20	0	0	<0.01
Alloy 4	Bal.	9.7	0.38	0.19	0	0	<0.01
Alloy 5	Bal.	10.3	0	0	0.57	1.31	<0.01
Alloy 6	Bal.	10.1	0.21	0.17	0.55	1.26	<0.01

2.2. Thermodynamic calculations

Thermo-Calc thermodynamic software (TCS Al-based Alloy Database-TCAL8) was used to analyse the equilibrium phase composition and solidification behaviour according to the Scheil-Gulliver model. The latter assumes that there is an infinitely fast diffusion in the liquid phase, but no diffusion takes place in the solid phase which allows for the local equilibrium at the liquid–solid interface once the phase has appeared. This approximation has been used to provide a reasonable estimate of solute profiles and describe phase formation in numerous studies including those concerning Al-Ce alloys [26–29].

2.3. Microstructure and phase composition characterization

Metallographic specimens were mounted and mechanically ground by SiC papers followed by cloth polishing in colloidal silica medium until a mirror finish was obtained. Specimens were etched using Keller's reagent to reveal the morphology of $Al_{11}Ce_3$ intermetallic. Grain size and eutectic spacing (λ) in all alloys were measured by analysing optical and SEM images in ImageJ software. For eutectic spacing, at least 100 measurements were taken and the average value is reported. Scanning electron microscopy (SEM, ZEISS Crossbeam 340) was used at 15 kV under backscattered mode to characterize the microstructure. A SEM attached EDS was used to confirm the composition of phases in alloys. Transmission electron microscopy (TEM) was used to characterize the precipitates in peak aged condition. TEM samples were prepared by mechanically grinding specimens to a thickness of ~150 μm followed by punching ϕ3mm discs. Discs were further ground to a thickness of ~40 μm using 2500 grid SiC paper followed by ion polishing to achieve electron transparency. For phase identification, X-ray diffraction (XRD) analysis was performed using a Bruker D8 Advance XRD instrument. The 2θ range for the analysis was set between 20° and 60°, with a step size of 0.01°/s.

2.4. Aging treatment

Samples from book mould castings were aged at 300 °C isothermally for a range of time duration from 1 h to 100 h. After each aging cycle, the samples were quenched in water. Vickers hardness tests were performed on the hot mounted samples using Wilson vo100 Vickers microhardness indenter by applying a load of 100 g and dwell time of 10 s. An average hardness value, for 10 indents taken at random positions, is reported. The ageing route that showed the best hardness was applied for HPDC cast tensile bars.

2.5. Tensile tests

A universal material testing machine (Instron ® 5560) equipped with Bluehill software was utilized for assessing yield and tensile strength. Testing procedures adhered to ASTM E8/E8M and ASTM E21 standards for room and elevated temperatures (150 °C and 300 °C), respectively. The alloys were held at the test temperature in the tensile test chamber

for 2 h. The ramp rate for room temperature tests was set at 1 mm/min, while the straining rate for high-temperature tests was maintained at 0.0002/s. Three samples were tested at each temperature, with the average value being reported.

3. Results

3.1. Microstructural analysis of gravity cast samples

Fig. 1 shows the optical micrographs of as-cast alloys produced by gravity casting. All alloys exhibit a typical near-eutectic microstructure with dominating (Al) dendrites and $Al_{11}Ce_3$ colonies, some dimensional differences can be seen due to the separate and combined addition of Zr, Sc, Mg and Si. Compared to the base Al-10Ce binary alloy (Fig. 1a), the addition of Zr and Sc does not seem to change the overall eutectic structure. However, compared to Alloy 2 which has a single Zr addition, combined Zr and Sc produced refined (Al) dendrites that can be attributed to the effect of Sc. Specifically, Alloy 2 has a grain size of 72 ± 14 μm, Alloy 4 (Fig. 1d) with 0.4 %Sc has an average grain size of 22 ± 4 μm. A similar refinement of α-Al dendrites due to Sc/Zr addition has been reported in the literature [30–33].

The more significant effect on microstructure can be seen by the addition of Mg and Si (Fig. 1e). A two-times increase in eutectic spacing in alloys 5 and 6 compared to other alloys can be seen probably due to the presence of additional phases. Minor presence of primary Sc/Zr-rich phases is detected in the most alloyed composition, Alloy 6 (Fig. 1f). This may account for the grain refinement effect and stipulate major dissolution of these elements in the matrix upon solidification. The composition of this primary phase was found to correspond to the $Al_3(Sc,Zr)$ phase by EDS analysis. SEM imaging using backscattered mode (BSE), EDS analysis and XRD were used to gain further insight into the present phases.

Fig. 2 shows the XRD spectrum of alloy 4 and alloy 6. Whereas both alloys show prominent peaks evidencing the presence of the $Al_{11}Ce_3$ phase, Alloy 6 shows an additional ternary phase, $(Al_xSi_{1-x})_2Ce$ which may show variable Al substitution for Si as was shown in [34]. We will stick to the designation of this phase as Al_2CeSi_2 which was previously reported in Al-Ce alloys with Si addition [27].

SEM analysis of Sc-free alloy (Alloy 2) reveals that the eutectic colonies consist of the fibrous and coarse lamellar $Al_{11}Ce_3$ (Fig. 3a) phase. Addition of 0.2 wt% Sc along with Zr increased the fibrous fraction and refined the lamellar intermetallics along the eutectic colonies (Fig. 3b). This effect has been enhanced with a further increase in Sc to 0.4 wt% in Alloy 4 (Fig. 3c) in agreement with previous studies [31,35]. Importantly, in the middle of the (Al) grains, the SEM analysis revealed the petal-shaped Sc- and Zr-rich particles confirmed to be $L1_2$-$Al_3(Sc, Zr)$ primary particles by EDS point analysis presented in Fig. 3d. The $Al_3(Sc, Zr)$ particles serve as potent heterogeneous nucleation sites for (Al) grains, owing to the similar lattice constants of Al crystal resulting in the observed grain refinement [36,37].

With the addition of Mg and Si, the morphology of the eutectic pool drastically changes from fibrous to lamellar. The colony boundaries contain even coarser lamellar particles with average composition of 25 at.% Al, 15 at.% and 60 at.% Ce obtained through EDS analysis (Fig. 4a), thus indicating the Al_2CeSi_2 phase. With the addition of all elements together, in Alloy 6 (Fig. 4b), the Sc brings a slight refining effect by bringing some fibrous fraction though the dominating structure is still relatively coarse. Some Sc-rich particles were found inside the eutectic mixture rather than inside the (Al) grain evidencing their possible local segregation limiting the eutectic growth (Fig. 4c). Similar observations were reported in a study by Mohammed et al. [10].

3.2. Thermal stability of alloys

Fig. 5 presents the evolution of the microhardness of alloys upon isothermal aging at 300 °C from 0 to 100 h. For as-cast condition, the Alloy 6 stands out as it has higher hardness (54 $HV_{0.1}$) compared to other alloys which is also reflected in the room temperature YS. Fig. 6 shows the room temperature YS and corresponding hardness of all alloys produced from HPDC, in as-cast condition. Such an improvement can be important for HPDC components which are often used without any heat treatment. An increase in strength can be seen with an increase in the amount of solute, specifically Sc and Zr. Moreover, the addition of Mg and Si resulted in the best yield strength among all as-cast alloys.

Upon heat treatment, the effect of precipitation was seen in all alloys apart from Alloy 1, which did not see any change even after 100 h at 300 °C. Alloy 2, which has 0.2 %Zr as an alloying element shows a marginal increase in the hardness ($HV_{0.1}$) after 24 h increasing from 36 to 45 and remains unchanged even after 100 h. On the contrary, Sc-containing alloys show a dramatic change in hardness after isothermal aging. Alloy 3 shows a jump from 41 to 77 after 1 h of heat treatment at 300°C and rises to 90 after 10 h. The same trend was observed in Alloy 4 which reached its peak hardness of 95 $HV_{0.1}$ after 10 h and showed a very slow decline up to 100 h. Alloy 6 showed a similar trend achieving a

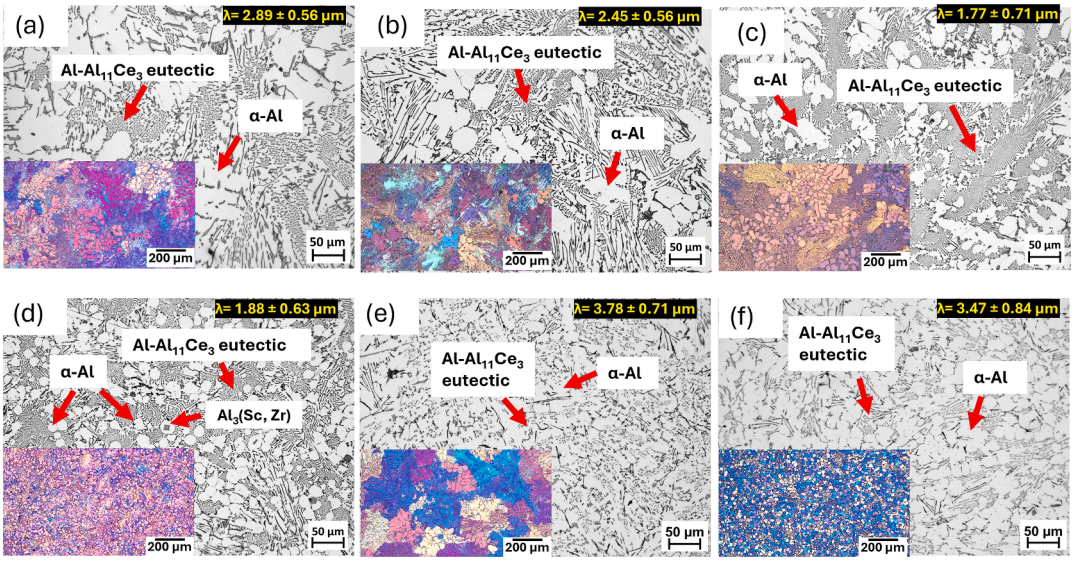

Fig. 1. Microstructures of as-cast alloys produced by gravity casting (a) Alloy 1 (b) Alloy 2 (c) Alloy 3 (d) Alloy 4 (e) Alloy 5 (f) Alloy 6. OM images taken with polarized light along with the numbers of eutectic spacing are given in the insets.

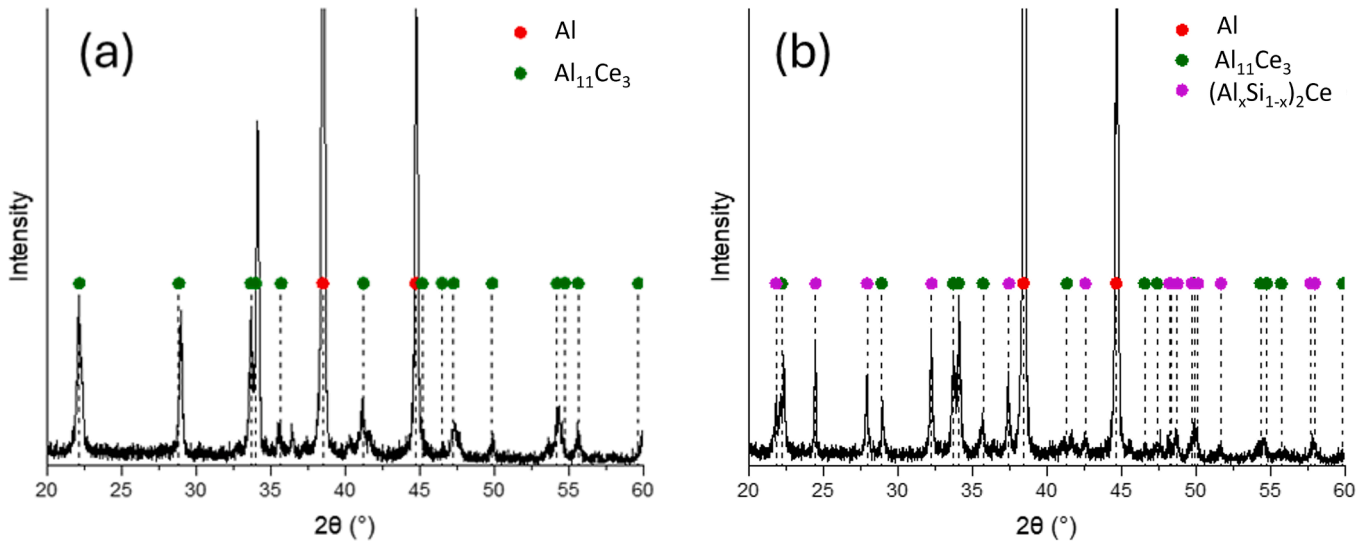

Fig. 2. XRD spectrum for as-cast alloy 4 (a) and alloy 6 (b).

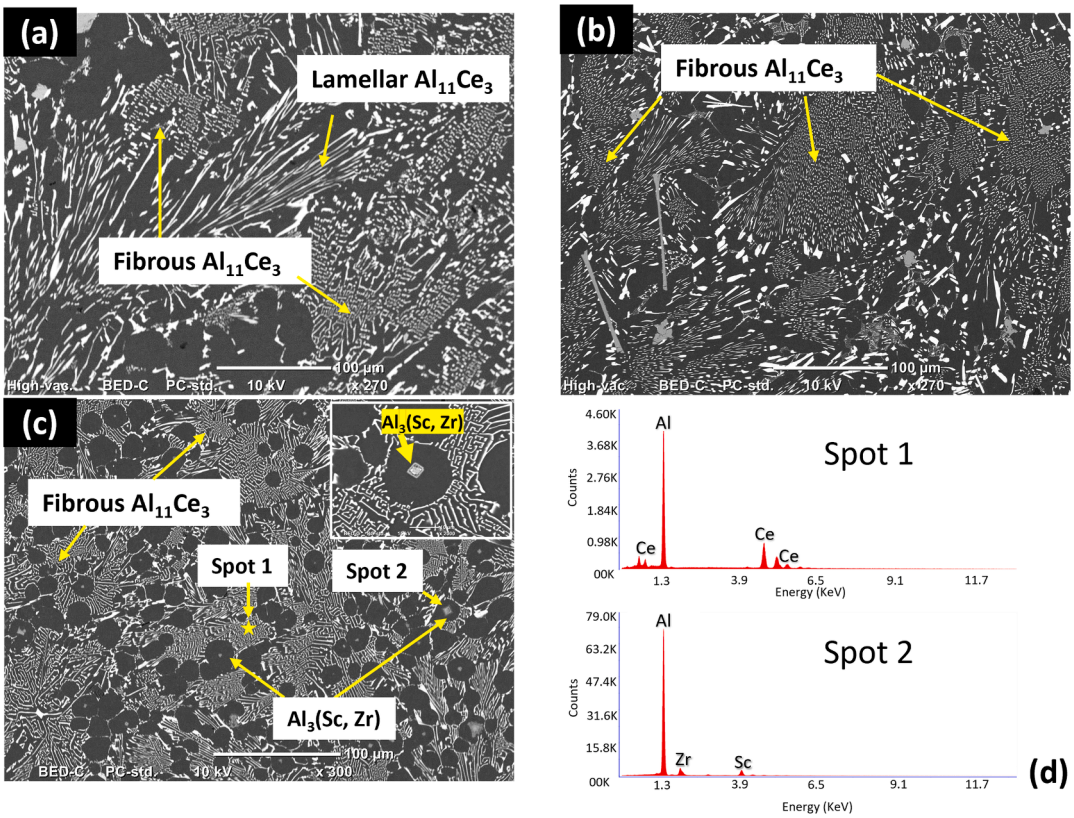

Fig. 3. SEM micrographs of as-cast alloys produced by gravity casting: (a) Alloy 2 (b) Alloy 3; SEM/EDS composition analysis of $Al_3(Sc, Zr)$ precipitates in (c) Alloy 4 (d) EDS analysis of spot 1 and 2.

peak hardness of 92 after 3 h and remaining unchanged throughout the aging process. One should note that an increase in Sc from 0.2 % to 0.4 % brought only a 5 $HV_{0.1}$ increment. A similar increment can be seen due to the addition of Mg and Si in the alloy containing 0.2 %Sc. Alloy 5 showed a higher hardness than Alloy 1 and 2 in as cast condition, due to effective Mg solid solution, and no considerable decline is observed upon aging indicating thermal stability of eutectic particles. Nevertheless, considering the price factor, more economical Sc alloying would be more beneficial for practical applications and the Alloy 6 stands out as Mg and Si are abundantly used in Al alloys and can be easily found in the raw materials including end-of-life scrap.

The bright field images of Alloy 3 (Fig. 7a) and 4 (Fig. 7d) aged at 300 °C, showing a high number density nanoscale particles in the Al matrix. HRTEM images indicate coherency of these particles with Al matrix in both alloys (Fig. 7b, e). Fast Fourier Transformation (FFT) obtained from the corresponding regions indicated by the square boxed in order to identify the precipitates (Fig. 7c, f). These particles were identified as ordered $L1_2$-$Al_3(Sc, Zr)$ precipitates by comparing the superlattice reflections in FFT pattern with theoretical pattern. The [0 0 1] zone axis has been confirmed as parallel to the incident beam for

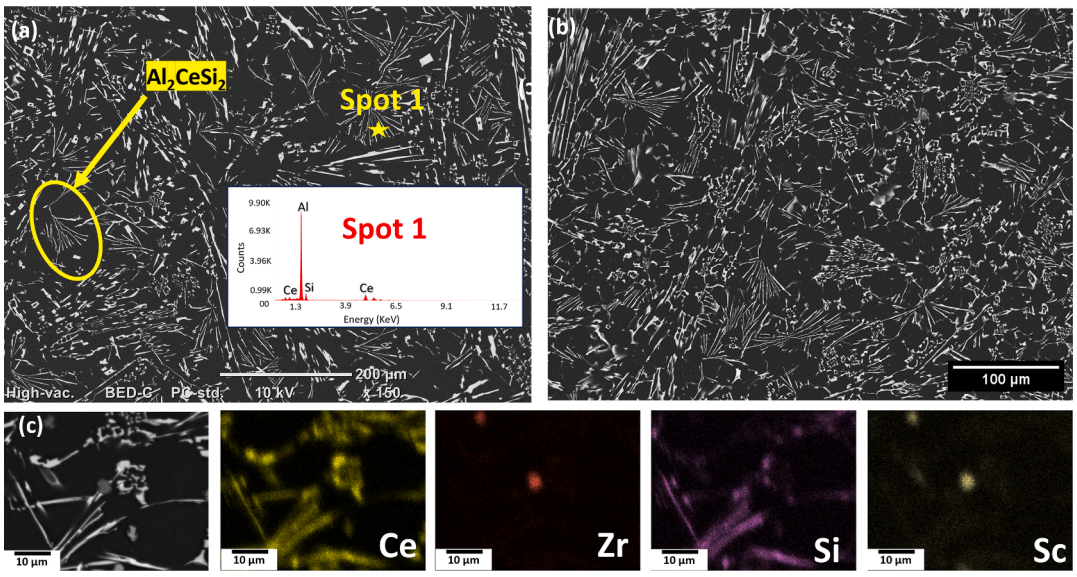

Fig. 4. SEM micrograph of as-cast (a) Alloy 5 highlighting the morphology of Al_2CeSi_2 phase with EDS spot analysis (b) Alloy 6 showing the morphology of eutectic phase (c) BSE image of a region in Alloy 6 with EDS elemental mapping.

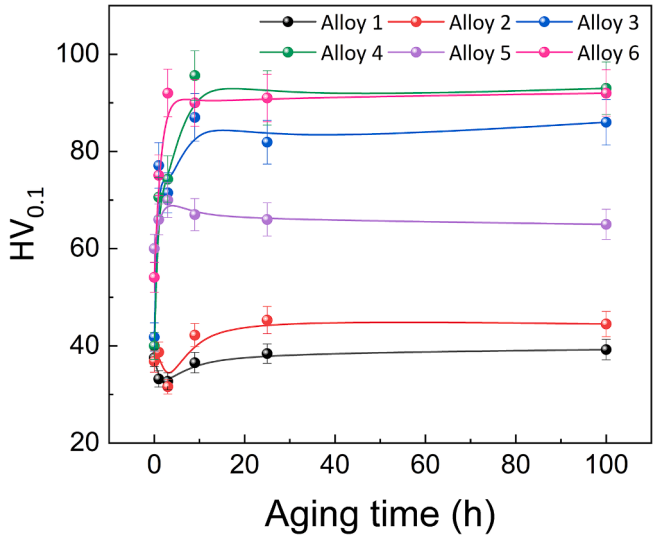

Fig. 5. Microhardness evolution of investigated alloys after isothermal aging at 300 °C with different holding times.

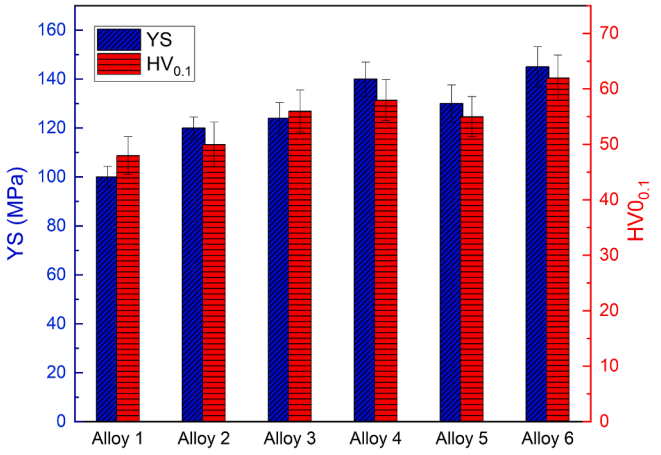

Fig. 6. Bar chart showing the hardness and YS of all as-cast alloys produced by HPDC.

both matrix and precipitates.

3.3. Mechanical behaviour of HPDC samples at room and elevated temperature

Fig. 8 shows the microstructures of all alloys produced by HPDC. The microstructures presented are at the location, half the radius of the tensile bar grip section. Intrinsic higher cooling rate offered in the HPDC process, compared to gravity die casting, brought an immense change in microstructure specifically in the refinement of dendrites and eutectic colonies. However, similarly to trends, observed for gravity casting, the effect of Sc is primarily about refining the microstructure by Al_3(Sc, Zr), whereas an increase in eutectic spacing can be seen with the addition of Mg and Si in alloys 5 and 6.

One should note that high cooling rates obtained by HPDC are prevailing the effect of Al_3(Sc, Zr) inoculants. Fig. 9 shows the grain structure of alloys intended for elevated temperature mechanical testing indicating similar grain size (15 ± 3 µm) independently on alloying addition. This means that the corresponding contribution to grain boundary strengthening is expected to be comparable for all alloys.

Fig. 10 shows the tensile properties of peak-aged HPDC samples (Alloys 1, 3, 5 and 6) at elevated temperatures. Peak ageing condition brought many thermally stable strengthening precipitates that allowed to largely maintain the strength at 150 °C at which alloy 6 again has the best strength properties compared to other alloys. However, an increase in test temperature significantly degraded the properties. The YS and UTS of Alloy 6 at 300 °C were measured to be ~90 and ~100 MPa showing the lowest retention as compared to Alloy 3 and 5, amongst all alloys, Alloy 4 shows a very minute deviation in the YS even at 300 °C. A comparison between the YS of present alloys and previously reported alloys along with the processing and testing temperatures is summarized in Table 2. To compare the high-temperature YS and elongation of present alloys with the previously studied Al alloys, a bar chart is presented in Fig. 10(c). It can be noticed that Al-Ce-Sc-Zr alloys produced by HPDC in the present study show a superior combination of strength and ductility at high temperature compared to conventional high-temperature Al-Si and Al-Cu alloys.

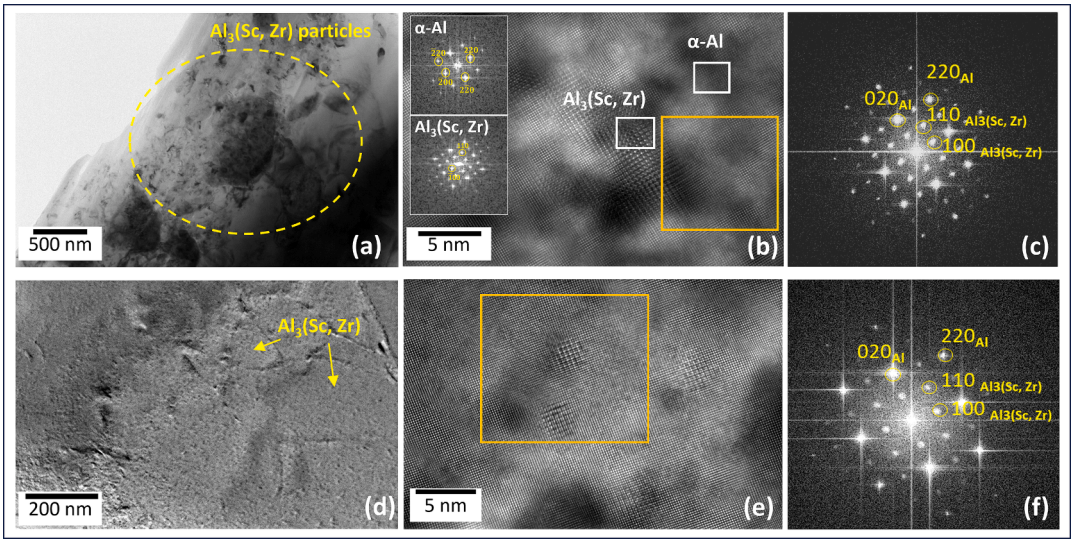

Fig. 7. TEM characterization of Alloy 3 and 4 peak aged at 300 °C: (a) bright field image of Alloy 3 showing dense distribution of $Al_3(Sc, Zr)$ precipitates; (b) HRTEM image of $Al_3(Sc, Zr)$ precipitates in Alloy 3 with corresponding Fast Fourier Transform (FFT) for Al matrix and $Al_3(Sc, Zr)$ precipitates as insets; (c) FFT pattern of Al and $Al_3(Sc, Zr)$ together in Alloy 3 (enclosed in orange square); (d) bright field image of Alloy 4; (e) HRTEM image of $Al_3(Sc, Zr)$ precipitates in Alloy 4; (f) FFT pattern of Al and $Al_3(Sc, Zr)$ together in Alloy 4 (enclosed in orange square). Incident beam was parallel to the [001] zone axis both for Al and $Al_3(Sc, Zr)$ precipitates. (For interpretation of the references to colour in this figure legend, the reader is referred to the web version of this article.)

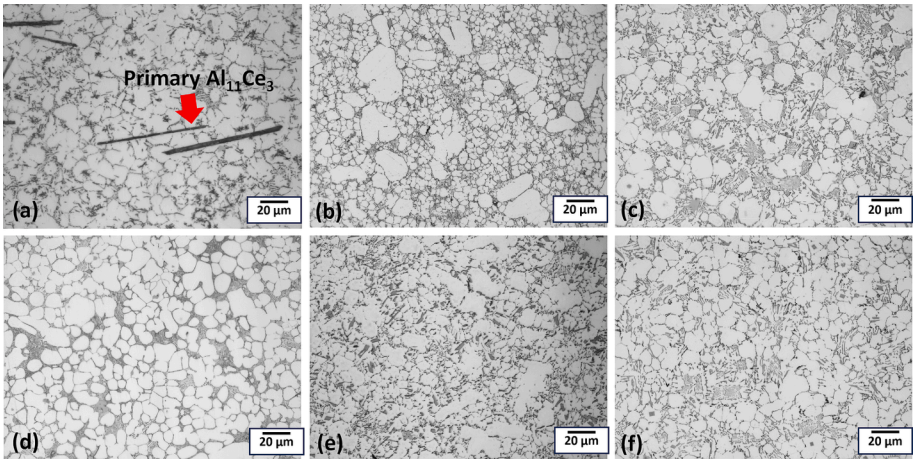

Fig. 8. Microstructures of as-cast alloys 1 (a), 2 (b), 3(c), 4(d), 5(e) and 6(f) produced by HPDC.

4. Discussion

4.1. Evolution of as-cast microstructure

Alloy 1 constitutes mainly (Al) matrix and $Al_{11}Ce_3$ phase uniformly distributed in the interdendritic region. The morphology of eutectic is lamellar throughout the sample. Addition of Sc and Zr compared to a single Zr addition leads to a refinement of (Al) dendrites and an increase in fibrous fraction in the eutectic pool at the expense of the boundary coarse lamellar particles. Formation of the Al_3Zr and $Al_3(Zr, Sc)$ phase during the early stages of solidification is evident due to a higher concentration of Sc and Zr. Due to heterogeneous nucleation potency of $Al_3(Sc, Zr)$ particles owing to the crystallographic relationship between particulate and matrix, refinement of grains is obtained in high Sc-containing alloy (Alloy 4). According to Turnbull and Vonnegut [52], the mismatch value is calculated by

$$\delta = \frac{\Delta a}{a_o} \quad (1)$$

where Δa is the mean difference between the lattice constants of matrix and substrate along the low index plane and a_o is the lattice constant of the matrix. $Al_3(Sc, Zr)$ phase has a cubic $L1_2$ structure with a = 4.100 Å and Al has a similar *fcc* structure with a = 4.059 Å, giving a mismatch of less than 1.25 %, indicating that $Al_3(Sc, Zr)$ phase can act as effective nucleating sites for Al.

The addition of Mg and Si modifies and makes the microstructure complex. In addition to eutectic $Al_{11}Ce_3$, the Al_2CeSi_2 phase is also present in Alloy 5 and 6. The morphology of the Al_2CeSi_2 phase is mostly lamellar protruding from the (Al) dendrites. To evaluate the phase composition evolution after solidification in Al-10Ce alloy by Mg, Si, Sc and Zr addition, CALPHAD calculations were conducted on Alloy 3 and 6. Fig. 9 shows the calculated non-equilibrium solidification path of Alloy 3 (Fig. 11a) and Alloy 6 (Fig. 11b). The formation of Al_3Zr and $Al_3(Zr, Sc)$ primary phases dominates the solidification curve before the appearance of Al. Usually, melt superheat before pouring and high cooling rates are applied for aluminium alloys containing Zr and Sc to form (Al) supersaturated solid solution. In the present study, the pouring temperature was 720 °C, which was lower than the liquidus temperatures predicted by the Scheil model for the given model alloys. One

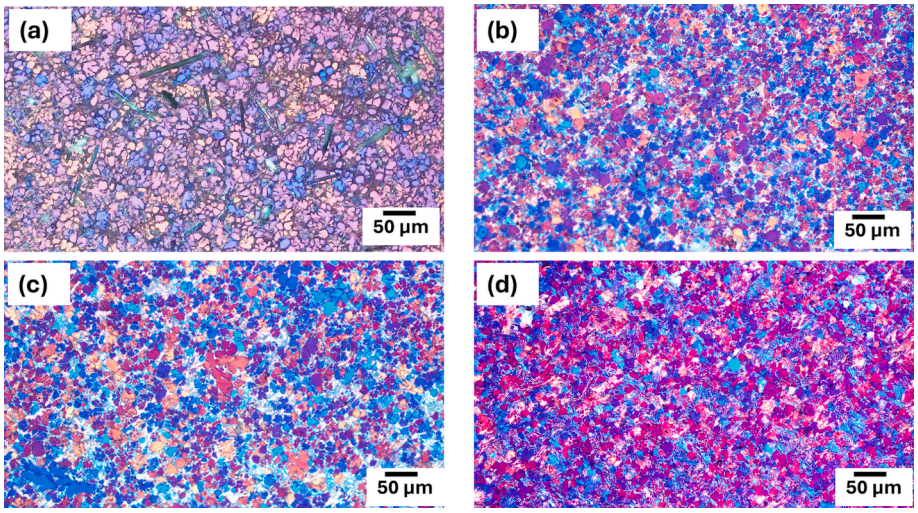

Fig. 9. Grain structure of alloys intended for mechanical testing at elevated temperature, in as cast condition: (a) Alloy 1, (b) Alloy 3, (c) Alloy 4 and (d) Alloy 6.

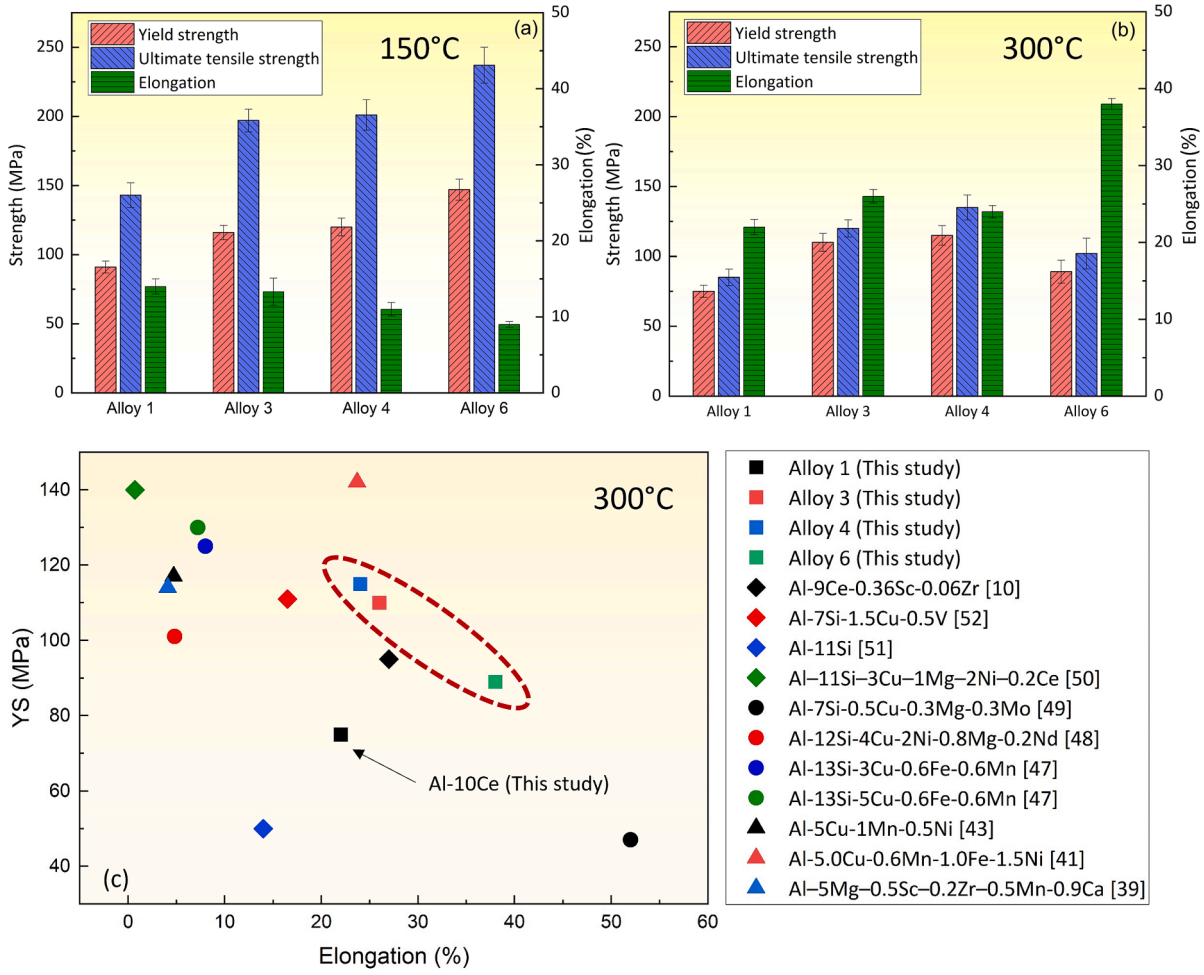

Fig. 10. Tensile properties of Alloys 1, 3, 4 and 6 in peak-aged condition (300 °C for 3 h for Alloy 6 and 10 h for Alloy 3 and 4) tested at (a) 150 °C and (b) 300 °C (c) comparison of mechanical properties of present alloys (highlighted in red ellipse) and previously reported die cast alloys at 300 °C. (For interpretation of the references to colour in this figure legend, the reader is referred to the web version of this article.)

should note that according to the calculation, the alloys fall in the hypoeutectic compositions. However, whereas a small fraction of the primary $Al_{11}Ce_3$ phase in the Alloy 3 alloy may form at 655 °C before L → Al + $Al_{11}Ce_3$ eutectic, the addition of Mg and Si modifies the phase equilibria. The Al_2CeSi_2 forms before Al_3Zr, and then keeps precipitating via binary L → Al + Al_2CeSi_2 eutectic and ternary L → Al + $Al_{11}Ce_3$ + Al_2CeSi_2 eutectic that agrees with the previously published data on Al-Ce-Si-Mg system [27]. The solidification terminates at 463 °C with the

Table 2
Mechanical properties of present alloys and previously reported alloys at room and elevated temperatures [10,13,38–51].

Alloy	Casting method, heat treatment conditions	Testing temperature (°C)	YS (MPa)	Reference
Alloy 1	HPDC, PA	150	91	This study
		300	75	
Alloy 3	HPDC, PA	150	116	This study
		300	110	
Alloy 4	HPDC, PA	150	120	This study
		300	115	
Alloy 6	HPDC, PA	150	147	This study
		300	89	
Al-9Ce-0.36Sc-0.06Zr	GC, PA	25	185	[10]
		300	95	
Al-7Si-1.5Cu-0.2Ti-0.5V	GC, AC	300	111	[50]
Al-11Si	GC, AC	25	125	[13]
		150	100	
		300	50	
Al–11Si–3Cu–1Mg–2Ni–0.2Ce	GC, T6	25	250	[49]
		250	200	
		300	140	
Al-7Si-0.5Cu-0.3Mg-0.3Mo	GC, T6	300	47	[48]
Al-12Si-4Cu-2Ni-0.8Mg-0.2Nd	GC, AC	25	196	[47]
		200	173	
		300	101	
Al-13Si-3Cu-0.6Fe-0.1Mn	GC, T6	25	210	[46]
		300	125	
Al-13Si-5Cu-0.6Fe-0.1Mn	GC, T6	25	280	[46]
		300	109	
Al-11Si-4Cu-0.2Fe-0.3Mn-0.2Zr	GC, T6	25	190	[44]
		300	105	
Al-4Cu	GC, T5	25	159	[45]
		300	93	
Al-4Cu-0.2Mn	GC, T5	25	158	[43]
		300	96	
Al-5Cu-1Mn-0.5Ni	GC, T6	25	170	[42]
		300	117	
Al-5Cu-0.4Mg	GC, T6	300	60	[41]
Al-5Cu-1.5Ni-0.2Mn0.2Zr	GC, T6	300	105	[41]
Al-5.0Cu-0.6Mn-1.0Fe-1.5Ni	SC, T7	250	188	[40]
		300	142	
Al-1.25Mn-1.28Mg-0.3Si-0.6Fe-0.3Mo	GC, PA	100	116	[39]
		200	111	
		300	85	
Al–5Mg–0.5Sc–0.2Zr–0.5Mn-0.9Ca	GC, PA	150	216	[38]
		250	160	
		300	114	
Al-1.25Mn-1.28Mg-0.3Si-0.6Fe	GC, PA	100	105	[39]
		200	100	
		300	78	

GC = Gravity casting, PA = Peak aged, SC = Squeeze casting.

formation of Mg_2Si and Al_3Mg_2 phases. However, in samples prepared from the HPDC route, the Al_3Mg_2 phase might not be expected in the microstructure as enrichment of Mg in the final solidification zone is retarded upon fast cooling during HPDC [53]. The Mg_2Si phase, on the other hand, is a well-known strengthening agent in AA6xxx alloys, which, however, could not be detected in the microstructure probably due to its minor amount compared to Ce-rich phases.

Though the cooling rate during HPDC casting is reasonable, the temperature can be decisive player for the appearance of primary intermetallic containing Zr and Sc. However, with increasing Sc, in Alloy 4, a considerable refinement in the $Al_{11}Ce_3$ is noticeable. In solid solution, Sc and Zr atoms tend to get adsorbed on the growing crystals of $Al_{11}Ce_3$ thus hindering the migration of Ce on $Al_{11}Ce_3$ [31]. This interaction effectively impedes the growth of the $Al_{11}Ce_3$ phase resulting in refined $Al_{11}Ce_3$.

4.2. Improvement of strength at room and high temperature

4.2.1. Room temperature mechanical properties in as-cast condition

The mechanisms influencing the room temperature strength primarily rely on the discussed solidification path and the observed grains and eutectic refining effects. The major contributor of strength in all studied alloys tested in as-cast condition includes solid solution strengthening, grain size strengthening and second phase strengthening. The theoretical strength of alloys at room temperature can be expressed as

$$\sigma_{ys} = \sigma_o + \Delta\sigma_{gb} + \Delta\sigma_{ss} + \Delta\sigma_{sp} \quad (2)$$

where, σ_{ys} is the theoretical strength, σ_o is the Peierls or friction stress (10 MPa for Al [54], $\Delta\sigma_{gb}$ is the contribution from grain boundary strengthening, $\Delta\sigma_{ss}$ is the strength contribution from solid solution and $\Delta\sigma_{sp}$ is the strength contribution from the load-bearing effect due to the lamellar $Al_{11}Ce_3$ phase. The strengthening from the $Al_{11}Ce_3$ phase can be estimated by following the shear lag theory [55]

$$\Delta\sigma_{sp} = 0.5\sigma_{int} f_{Al_{11}Ce_3}(2+S) \quad (3)$$

where, σ_{int} is the interface strength of matrix/reinforcement, $f_{Al_{11}Ce_3}$ is the volume fraction and S is the aspect ratio (length/width) of the $Al_{11}Ce_3$ eutectic phase. The volume fraction of $Al_{11}Ce_3$ in all alloys was calculated using the CALPHAD method with an average value of ~10 %. S is calculated by analysing the SEM images in ImageJ software. However, the average value of S in all alloys ranges from 6 to 10. A rough estimation of S is taken to be 8 in all alloys. Since σ_{int} is hard to measure,

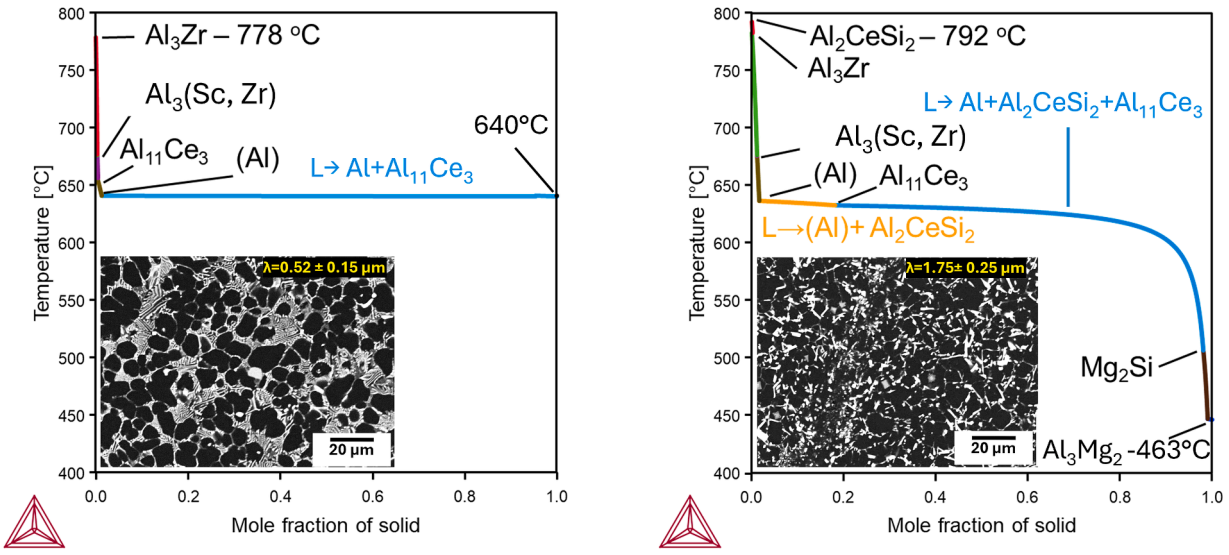

Fig. 11. Non-equilibrium solidification curves calculated using Scheil-Gulliver model for (a) Alloy 3 and (b) Alloy 6. The SEM images and eutectic spacing of the corresponding alloys are given in the insets.

we assume that the interface is identical to the Al-SiC composite with $\sigma_{int} = 133$ MPa, similar assumptions were made to calculate the load-bearing effect in Ref [30]. Substituting $\sigma_{int} = 133$ MPa in Eq. (4), the contribution from load bearing effect is estimated to be 67 MPa in all alloys. The calculated value is a rough theoretical estimate possible to be contributed by $Al_{11}Ce_3$. However, the observed eutectic refinement may bring differences towards further strength improvement observed during the tensile test due to an increase in fibrous fraction observed with an increase in Sc (e.g. see Fig. 3).

Secondly, the contribution from grain size can be given by the Hall-Petch relationship [56,57]

$$\Delta\sigma_{gb} = K/\sqrt{d} \tag{4}$$

where K is the Hall-Petch constant, and d is the average grain diameter. For Sc-containing HPDC samples, the observed d is about ~15 μm in all alloys, which is within the range of the commonly observed grain size in Al alloys fabricated through HPDC [58,59]. K value of Al is taken to be 80 MPa·$\mu m^{1/2}$ [60]. Equation (5) yields a value of $\Delta\sigma_{gb} = 20$ MPa. The larger grains observed in Sc-free alloys would change the grain size contribution respectively explaining their lower strength.

In as-cast condition obtained after fast cooling by HPDC, the matrix supersaturation and solid solution strengthening plays a significant role as well. Though we could see a minor presence of primary Zr- and Sc-rich phases, their amount was limited due to a high casting temperature allowing for the elements to dissolve and stay in the matrix. The composition of the liquid phase and amount of primary intermetallics were calculated at casting temperature, 720 °C using Thermo-Calc software (Table 3). Almost all Sc added in the alloy dissolves in the melt at this temperature, whereas for Zr, about 0.06 wt% and small Sc form primary intermetallics which amount was estimated to be less than 0.1 vol%, in agreement with microstructure observations.

Table 3
Calculated composition of the liquid at 720 °C and fraction of phases in the melt.

Alloy	Temp (°C)	Sc in Liquid, wt.%	Zr in Liquid, wt.%	$Al_3(Sc, Zr)$, vol.%	Al_2CeSi_2, vol.%
Alloy 3	720	0.19	0.097	0.14	–
Alloy 4	720	0.35	0.09	0.03	–
Alloy 6	720	0.19	0.09	0.14	0.75

The strength contribution from solid solution in Al alloys is given by the relation [61]

$$\Delta\sigma_{ss} = M\left(\frac{3}{8}\right)^{\frac{2}{3}}\left(\frac{1+\vartheta}{1-\vartheta}\right)^{\frac{4}{3}}\left(\frac{w}{b}\right)^{\frac{1}{3}}\mu|\varepsilon|^{\frac{4}{3}}c^{\frac{2}{3}} \tag{5}$$

where M is Taylor factor (3.06 for Al), μ is the shear modulus of Al (26.5GPa) [62], υ is the Poisson's ratio (0.347) [62], $w = 5b$, ε is the misfit strain which is related to the difference in the interatomic distance (1.25 % for Sc and 1.23 % for Zr [61]) and c is the atomic % of solute in the matrix. Equation (6) yields the value of $\Delta\sigma_{ss}(Sc) = 7$MPa, $\Delta\sigma_{ss}(Zr) = 4$MPa in Alloy 3 whereas in Alloy 4, $\Delta\sigma_{ss}(Sc) = 14$MPa, $\Delta\sigma_{ss}(Zr) = 4$MPa. As-cast alloy 4 is stronger than alloy 3 only due to higher Sc content whereas alloy 6 may be even harder due to possible Mg solute. The amount of Mg and Si in the matrix depends on their distribution between the matrix and intermetallic which is more challenging considering the complex phase composition. However, compared to Si, depleted in (Al) due to the formation of the Al_2CeSi_2 phase, a larger Mg in solid solution can be expected in Alloy 6 after casting. Hu et al. [25] evaluated the influence of Mg on the strength of Al-8Ce alloy cast through HPDC. Mg atoms were found to be present in the solid solution owing to the dramatically higher cooling rate in HPDC and no Mg-containing compounds were formed. The addition of Mg enhanced the YS increased from ~92 MPa for Al-8Ce to 115 MPa for Al-8Ce-0.75 Mg alloy. A simpler form of Equation (6) can be used to estimate the value of $\Delta\sigma_{ss}(Mg) = k\,c^{2/3}$, where k (MPa/wt.%$^{2/3}$) is a scaling factor with a value of 29 MPa /wt.%$^{2/3}$ [63], yielding a value of ~33 MPa accounting for the maximum possible increment in case all Mg (1.2 wt%) enters the (Al) matrix. This theoretical strength contribution is close to the actual difference in as-cast YS values between alloys 1 and 5 and alloys 3 and 6.

HPDC components are frequently used in as-cast condition. It was shown by the present study that even as-cast strength can be improved without any heat treatment by the addition of Sc and Zr as well as by aiding some solid solution effect of Mg, whereas Si can be considered as a neutral impurity as it does not contribute to strength.

4.2.2. *Effect of elevated temperature on mechanical properties*

As can be seen from Fig. 10, alloys 3 and 4 show minimal degradation in strength at high temperatures whereas alloy 6 retains high properties at 150 °C but degrades significantly at 300 °C. The major contribution to the retention of the properties is brought by the $Al_3(Sc, Zr)$ nano dispersoids precipitated during the aging operations. The dispersoids

impede dislocation movement, increasing YS. Two mechanisms are prominent in precipitation strengthening, firstly the pinning of dislocation (shearing of precipitates) and secondly, the bypassing of dislocations known as the Orowan looping mechanism. The significant contribution of Al_3(Sc, Zr) nanoprecipitates is reflected in the hardness response of Sc and Zr-containing alloys. No significant coarsening of precipitates and loss in hardness with time at 300 °C could be seen even in Si-containing alloys probably due to no interaction between Si and Al_3(Sc, Zr). Such an interaction has been reported for the Al-Si alloys doped with Sc and (Al, Si)$_3$Sc may have only partial coherence with the matrix thus reducing the strength contribution [64]. In the present study, such a phase is not forming as the Al_2Ce2Si_2 phase is more thermodynamically stable across the studied temperature range.

Nevertheless, for Mg and Si-containing alloys, the strengthening mechanism is obviously not limited to Al_3(Sc, Zr) dispersoids. As can be seen from Fig. 5, alloy 6, shows the same hardness as alloy 4 after ageing for 100 h at 300 °C, whilst having two times smaller Sc content. Considering that the calculated solid solubility of Mg in Al at 300 °C is 1 wt% (Table 4) and the samples were quenched after ageing, the increment in room temperature properties of the aged alloy 6 can be attributed to Mg solute atoms supersaturated in (Al). A simple calculation performed similarly to the as-cast condition showed that solid solution strengthening contribution is equal to 29 MPa. According to the well-known empirical relationship $YS = 3\ HV$, the calculated $HV_{0.1}$ increment due to 1 wt.%Mg in Al is 8 $HV_{0.1}$ which coincides well with the difference in $HV_{0.1}$ between alloy 3 and 6 after the thermal stability test.

Although, Alloy 6 shows appreciable thermal stability, its mechanical behaviour at high temperatures was found to be different at 150 °C and 300 °C. The addition of Mg and Si is common for heat-treatable AA6xxx aluminium alloys, and their performance is directly correlated with the content of these elements. Therefore, equilibrium isothermal sections calculated at 150 and 300 °C for the Al-Ce-Zr-Sc-Si-Mg system are given in Fig. 12. These sections show that Alloy 6 may fall in a different phase region depending on the temperature, Mg and Si content which may all potentially affect mechanical properties.

At 150 °C, the alloy is in the $Al_{11}Ce_3$ + Al_3(Zr, Sc) + Mg_2Si + (Al) phase field which should benefit from the maximum Mg_2Si and Al_3(Sc, Zr) fractions bringing the corresponding strengthening effect, similar to the typical ageing of AA6xxx alloys. This effect can be possible in alloys with Mg:Si ratio of about 2:1 in the event of Mg- and Si-supersaturated (Al) matrix. However, this scenario could not be realized because the alloys were peak aged at 300 °C and quenched bringing a Si-depleted but Mg-rich solid solution. Apparently, from Fig. 8 it can be seen that all alloys perform their best mechanical properties in this study at 150 °C, which is the routine ageing temperature maximum operational temperature for many heat-treatable aluminium alloys due to limited coarsening of precipitates and limited mobility of solutes. Therefore, similar to the room temperature hardness after peak ageing, the excellent performance of alloy 6 at 150 °C can be attributed to solid solution strengthening.

Table 4
Calculated phase composition of the experimental alloys at 300 °C.

Alloy	Phase	Q_m (wt. %)	Q_v (vol. %)	Chemical composition (wt.%)				
				Ce	Sc	Zr	Si	Mg
Alloy 1	(Al)	82.9	88.3	0	–	–	–	–
	$Al_{11}Ce_3$	17.1	11.7	58.6	–	–	–	–
Alloy 3	(Al)	82.0	87.5	0	0	0	–	–
	$Al_{11}Ce_3$	17.1	11.8	58.6	0	0	–	
	Al_3(Zr, Sc)	0.9	0.8	0	21.4	21.3	–	–
Alloy 4	(Al)	81.4	86.9	0	0	0		
	$Al_{11}Ce_3$	17.1	11.8	58.6	0	0	–	–
	Al_3(Zr, Sc)	1.5	1.3	0	26.7	13.3	–	–
Alloy 6	(Al)	81.4	86.7	0	0	0	0	1.0
	$Al_{11}Ce_3$	15.5	10.6	58.6	0	0	0	0
	Al_2CeSi_2	1.5	1.0	60.3	0	0	24.2	0
	Mg_2Si	0.6	0.9	0	0	0	36.6	63.4
	Al_3(Zr, Sc)	0.9	0.8	0	21.3	21.3	0	0

A further increase in temperature causes stronger thermal vibration amplitude and a decrease in bonding force between atoms, hence, bringing to the matrix. Alloy 6 saw a significant degradation in strength and an increase in relative elongation at 300 °C compared to a lower temperature and other alloys. At 300 °C the alloy is well falling in the Al_2CeSi_2 + $Al_{11}Ce_3$ + Al_3(Sc, Zr) + Mg_2Si + (Al) region which is equilibrium even at significant Mg excess The Al_2CeSi_2 phase is a significant solute consumer negatively affecting the Mg-Si precipitation hardening. As can be seen from the equilibrium phase composition at 300 °C (Table 4), the addition of Zr and Sc neither influence the fraction of Ce-rich and Mg_2Si phases nor their composition, thus it can be expected that the strengthening contribution of the Al_3(Zr, Sc) phase depends only on whether they appear as dispersoids or primary intermetallic. Both variants were found in the microstructure of alloy 6 as it was age-hardened with temperature and showed appreciable thermal stability whilst having refined grain structure due to observed primary particles. Whereas some Si can be bound in a small fraction of the Mg_2Si phase, their possible contribution to strength is negligible due to unavoidable ripening at 300 °C. For this reason, Mg-Si precipitation is considered not to affect either room temperature or high-temperature performance of aged samples.

Thus, degraded properties can be related to either significantly changed eutectic structure or to loss in the efficiency of Mg solute obstacles. According to [65], the solid solution strengthening in Al-Mg binary alloy with increasing temperature due to rapid recovery. A limited solid solution strengthening was reported for Al-Ca-Mg-Sc alloys during testing at 300 °C [66]. In Odoh et al. [67], the flow stress was increasing with Mg content, but such an increase was significantly reduced due to an increase in solute diffusivity at high temperatures. Such an effect is hardly avoidable at high temperatures, making the doping of the Al-Ce-Sc-Zr alloys with Mg less effective. A significantly increased eutectic spacing has been evidenced in the present study. According to [68], describing the influence of eutectic spacing on yield strength using the classic Brown model and Taylor-Orowan's equation, the strengthening grows with the smaller eutectic spacing or denser distribution of the second phase, since it relates to the characteristic length of the slip band in the matrix. With all alloys having identical grain size, the eutectic spacing changed significantly only for alloy 6 which likely caused a larger exposure of the soft matrix to mechanical deformation and a significant degradation in strength.

5. Conclusion

The present study presents the influence of Mg, Sc, Zr and Si on the microstructure of hypoeutectic Al-10Ce alloy. Thermal stability and mechanical strength of produced Alloys were examined in as-cast condition at room temperature and in heat treated condition at elevated temperatures. The key observations can be presented as followed.

1. A series of Al-Ce alloys with various composition of Mg, Si, Zr and Sc were cast using permanent mould and high-pressure die-casting methods. Al_3(Sc, Zr) particles form in the melt and act as the preferential nucleation sites for the α-Al grains resulting the effective grain refinement.
2. Upon ageing, dramatic elevation in hardness during ageing at 300 °C is recorded in Sc, Zr containing alloys pertaining to the formation of Al_3(Sc, Zr) nanoprecipitates from the supersaturated solid solution in

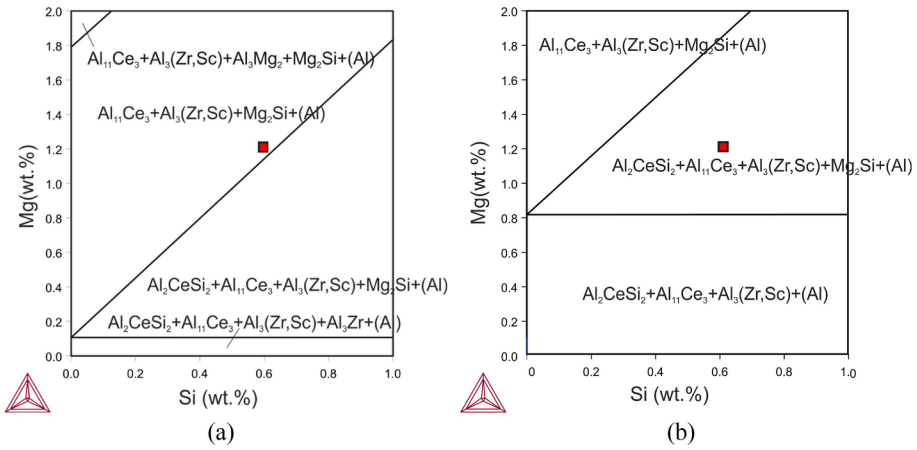

Fig. 12. Isothermal sections of Al-Ce-Zr-Sc-Si-Mg system at 10 wt.%Ce, 0.2 wt. %Sc, 0.2wt.%Zr calculated at 150 °C (a) and 300 °C (b): red square shows the Alloy 6 position. (For interpretation of the references to colour in this figure legend, the reader is referred to the web version of this article.)

the matrix. Due to these nanoprecipitates, the hardness is being maintained after ageing for 100 h.

3. As-cast Alloy 6 shows the highest YS of 147 MPa at room temperature testing due to strengthening sources from Sc, Zr, Mg and Si additions. In peak-aged condition also, this alloy shows superior strength at elevated temperature testing condition (150 °C). However, YS decline dramatically to 89 MPa at 300 °C. Whereas Alloy 4 shows higher strength of 115 MPa at 300 °C. At room temperature, solution strengthening from Mg is the dominant contributor of strength whereas at higher temperatures, Al_3(Sc, Zr) nanoprecipitates are the biggest contributor of strength.

CRediT authorship contribution statement

Shishir Keerti: Writing – original draft, Methodology, Investigation, Formal analysis, Data curation. **Pavel Shurkin:** Writing – review & editing, Software, Investigation, Formal analysis. **Qing Cai:** Methodology, Investigation, Formal analysis. **Hari Babu Nadendla:** Writing – review & editing, Visualization, Supervision, Methodology, Funding acquisition, Formal analysis, Conceptualization. **Animesh Mandal:** Writing – review & editing, Visualization, Project administration, Funding acquisition, Conceptualization.

Declaration of competing interest

The authors declare the following financial interests/personal relationships which may be considered as potential competing interests: Shishir Keerti reports financial support was provided by Ministry of Human Resource Development, Government of India. Hari Babu Nadendla reports financial support was provided by Engineering and Physical Sciences Research Council. If there are other authors, they declare that they have no known competing financial interests or personal relationships that could have appeared to influence the work reported in this paper.

Acknowledgements

The authors would like to acknowledge funding from The Scheme for Promotion of Academic and Research Collaboration (SPARC), an initiative of the Ministry of Human Resource Development, Government of India (SPARC/2018-2019/P744/SL) and, project EP/Y025016/1 for partial funding.

Data availability

Data will be made available on request.

References

[1] B.J.E. Dorn, Some fundamental experiments on high temperature creep, J. Mech. Phys. Solids 8 (1954) 85–116, https://doi.org/10.1016/0022-5096(55)90054-5.
[2] R.L. Carlson. Investigation of compressive-creep properties of Aluminium columns at elevated temperatures, Battelle Memorial Institute (1952). doi: https://apps.dtic.mil/sti/tr/pdf/ADA076046.pdf.
[3] E. Georgantzia, M. Gkantou, G.S. Kamaris, Aluminium alloys as structural material: a review of research, Eng. Struct. 227 (2021), https://doi.org/10.1016/j.engstruct.2020.111372.
[4] Z.C. Sims, D. Weiss, S.K. Mccall, M.A. Mcguire, R.T. Ott, T.O.M. Geer, O. Rios, P.A. E. Turchi, Cerium-based, intermetallic-strengthened aluminum casting alloy: high-volume co-product development, JOM 68 (2016) 1940–1947, https://doi.org/10.1007/s11837-016-1943-9.
[5] Z.C. Sims, O.R. Rios, D. Weiss, P.E.A. Turchi, A. Perron, J.R.I. Lee, T. Tian, J. A. Hammons, M. Bagge-hansen, T.M. Willey, K. An, Y. Chen, A.H. King, S.K. Mccall, High performance aluminum-cerium alloys for high-temperature applications, JOM 68 (2016) 1940–1947, https://doi.org/10.1007/s11837-016-1943-9.
[6] F. Czerwinski, Cerium in aluminum alloys, J. Mater. Sci. 55 (2020) 24–72, https://doi.org/10.1007/s10853-019-03892-z.
[7] C. Weiping, Diffusion of cerium in the aluminium lattice, J. Mater. Sci. Lett. 16 (1997) 1824–1826, https://doi.org/10.1023/A:1018572803223.pdf.
[8] H. Okamoto, Al-Ce (Aluminum-Cerium), 32 (2011) 11669. doi: 10.1007/s11669-011-9914-x.
[9] Y. Liu, R.A. Michi, D.C. Dunand, Cast near-eutectic Al-12 . 5 wt .% Ce alloy with high coarsening and creep resistance, Mater. Sci. Eng. A 767 (2019) 138440, https://doi.org/10.1016/j.msea.2019.138440.
[10] A.A. Mohammed, S. Chankitmunkong, S. Wang, D.G. Eskin, U. Patakham, C. Limmaneevichitr, P. Pandee, Enhancing ambient and elevated temperature performance of hypoeutectic Al–Ce cast alloys by Al3(Zr, Sc) precipitate, J. Mater. Res. Technol. 28 (2024) 1188–1197, https://doi.org/10.1016/j.jmrt.2023.12.021.
[11] F. Czerwinski, B.S. Amirkhiz, On the Al-Al11Ce3 eutectic transformation in aluminum-cerium binary alloys, Materials 13 (2020) 1–27, https://doi.org/10.3390/ma13204549.
[12] D. Weiss, Castability and Characteristics of High Cerium Aluminum Alloys, in: Advanced Casting Technologies, InTech, 2018. doi: 10.5772/intechopen.72830.
[13] G. Rajaram, S. Kumaran, T.S. Rao, High temperature tensile and wear behaviour of aluminum silicon alloy, Mater. Sci. Eng. A 528 (2010) 247–253, https://doi.org/10.1016/j.msea.2010.09.020.
[14] D. Weiss, Improved high-temperature aluminum alloys containing cerium, J. Mater. Eng. Perform. 28 (2019) 1903–1908, https://doi.org/10.1007/s11665-019-3884-2.
[15] L. Wang, R. Qi, B. Ye, Communication improved tensile strength of Al-5Ce alloy by permanent magnet stirring, Metall. Mater. Trans. A 51 (2020) 1972–1977, https://doi.org/10.1007/s11661-020-05723-2.
[16] K.E. Knipling, D.C. Dunand, D.N. Seidman, Nucleation and precipitation strengthening in dilute Al-Ti and Al-Zr alloys, Metall. Mater. Trans. A 38 (2007) 2552–2563, https://doi.org/10.1007/s11661-007-9283-6.
[17] K.E. Knipling, D.C. Dunand, D.N. Seidman, Criteria for developing castable, creep-resistant aluminum-based alloys-a review, Int. J. Mater. Res. 97 (2006) 246–265, https://doi.org/10.1515/ijmr-2006-0042.
[18] C.B. Fuller, D.N. Seidman, D.C. Dunand, Mechanical properties of Al(Sc,Zr) alloys at ambient and elevated temperatures, Acta Mater. 51 (2003) 4803–4814, https://doi.org/10.1016/S1359-6454(03)00320-3.
[19] N.Q. Vo, D.C. Dunand, D.N. Seidman, Improving aging and creep resistance in a dilute Al-Sc alloy by microalloying with Si, Zr and Er, Acta Mater. 63 (2014) 73–85, https://doi.org/10.1016/j.actamat.2013.10.008.
[20] T. Dorin, S. Babaniaris, L. Jiang, A. Cassel, A. Eggeman, J. Robson, Precipitation sequence in Al-Sc-Zr alloys revisited, Materialia (Oxf) 26 (2022), https://doi.org/10.1016/j.mtla.2022.101608.

[21] A. Tolley, V. Radmilovic, U. Dahmen, Segregation in Al3(Sc,Zr) precipitates in Al-Sc-Zr alloys, Scr. Mater. 52 (2005) 621–625, https://doi.org/10.1016/j.scriptamat.2004.11.021.

[22] L. Wang, B. Ye, Y. Bai, B. Zhao, W. Ding, Effect of Zr and Sc micro-additions on the microstructure and mechanical properties of as-cast Al-5Ce alloy, Mater. Sci. Eng.: A 822 (2021) 141654, https://doi.org/10.1016/j.msea.2021.141654.

[23] M. Yi, P. Zhang, C. Yang, P. Cheng, S. Guo, G. Liu, J. Sun, Improving creep resistance of Al-12 wt.% Ce alloy by microalloying with Sc, Scr. Mater. 198 (2021) 113838, https://doi.org/10.1016/j.scriptamat.2021.113838.

[24] Z.C. Sims, D. Weiss, S.K. McCall, M.A. McGuire, R.T. Ott, T. Geer, O. Rios, P.A. E. Turchi, Cerium-based, intermetallic-strengthened aluminum casting alloy: high-volume co-product development, JOM 68 (2016) 1940–1947, https://doi.org/10.1007/s11837-016-1943-9.

[25] B. Hu, B. Quan, D. Li, X. Wang, Z. Li, X. Zeng, Solid solution strengthening mechanism in high pressure die casting Al–Ce–Mg alloys, Mater. Sci. Eng. A 812 (2021), https://doi.org/10.1016/j.msea.2021.141109.

[26] A.E. Perrin, R.A. Michi, D.N. Leonard, K.D. Sisco, A.J. Plotkowski, A. Shyam, J. D. Poplawsky, L.F. Allard, Y. Yang, Effect of Mn on eutectic phase equilibria in Al-rich Al-Ce-Ni alloys, J Alloys Compd 965 (2023), https://doi.org/10.1016/j.jallcom.2023.171455.

[27] F. Czerwinski, B. Shalchi Amirkhiz, Aluminum cast alloys based on the Al–Ce–Si–Mg system: an influence of silicon on crystallization, phase composition, and tensile properties, Metall. Mater. Trans. A Phys. Metall. Mater. Sci. 53 (2022) 4233–4246, https://doi.org/10.1007/s11661-022-06812-0.

[28] K. Sisco, A. Plotkowski, Y. Yang, D. Leonard, B. Stump, P. Nandwana, R.R. Dehoff, S.S. Babu, Microstructure and properties of additively manufactured Al–Ce–Mg alloys, Sci. Rep. 11 (2021), https://doi.org/10.1038/s41598-021-86370-4.

[29] H. Hyer, A. Mehta, K. Graydon, N. Kljestan, M. Knezevic, D. Weiss, B. McWilliams, K. Cho, Y. Sohn, High strength aluminum-cerium alloy processed by laser powder bed fusion, Addit. Manuf. 52 (2022), https://doi.org/10.1016/j.addma.2022.102657.

[30] J. Xiao, Z. Zhang, J. Ye, Z. Wang, K. Dai, J. Li, R. Guan, Microstructure and property optimization of Al–8Ce alloys: electromagnetic stirring and Sc–Zr microalloying, J. Mater. Res. Technol. 28 (2024) 3133–3143, https://doi.org/10.1016/j.jmrt.2023.12.253.

[31] J. Ye, K. Dai, Z. Wang, J. Chen, M. Gao, R. Guan, Beneficial effects of Sc/Zr addition on hypereutectic Al–Ce alloys: modification of primary phases and precipitation hardening, Mater. Sci. Eng. A 835 (2022), https://doi.org/10.1016/j.msea.2022.142611.

[32] S. Zhou, Z. Zhang, M. Li, D. Pan, H. Su, X. Du, P. Li, Y. Wu, Effect of Sc on microstructure and mechanical properties of as-cast Al-Mg alloys, Mater. Des. 90 (2016) 1077–1084, https://doi.org/10.1016/j.matdes.2015.10.132.

[33] W. Wang, Q. Pan, F. Jiang, Y. Yu, G. Lin, X. Wang, J. Ye, D. Pan, Z. Huang, S. Xiang, J. Li, B. Liu, Microstructure evolution and performances of Al-0.7Mg-0.6Si-0.2Ce-X (X=Sc, Y and Zr) alloys with high strength and high electrical conductivity, J. Alloys Compd. 895 (2022) 162654, https://doi.org/10.1016/j.jallcom.2021.162654.

[34] J. Gröbner, D. Mirković, M. Mirković, R. Schmid-Fetzer, Thermodynamic aspects of the constitution, grain refining, and solidification enthalpies of Al-Ce-Si alloys, Metall. Mater. Trans. A 35 (2004) 3349–3362, https://doi.org/10.1007/s11661-004-0172-y.

[35] L. Wang, B. Ye, Y. Bai, B. Zhao, W. Ding, Effect of Zr and Sc micro-additions on the microstructure and mechanical properties of as-cast Al-5Ce alloy, Mater. Sci. Eng. A 822 (2021), https://doi.org/10.1016/j.msea.2021.141654.

[36] S. Costa, H. Puga, J. Barbosa, A.M.P. Pinto, The effect of Sc additions on the microstructure and age hardening behaviour of as cast Al-Sc alloys, Mater. Des. 42 (2012) 347–352, https://doi.org/10.1016/j.matdes.2012.06.019.

[37] K. Venkateswarlu, L.C. Pathak, A.K. Ray, G. Das, P.K. Verma, M. Kumar, R. N. Ghosh, Microstucture, tensile strength and wear behaviour of Al-Sc alloy, Mater. Sci. Eng. A 383 (2004) 374–380, https://doi.org/10.1016/j.msea.2004.05.075.

[38] H. Du, S. Zhang, B. Zhang, X. Tao, Z. Yao, N. Belov, S. van der Zwaag, Z. Liu, Ca-modified Al–Mg–Sc alloy with high strength at elevated temperatures due to a hierarchical microstructure, J. Mater. Sci. 56 (2021) 16145–16157, https://doi.org/10.1007/s10853-021-06310-5.

[39] K. Liu, H. Ma, X.G. Chen, Enhanced elevated-temperature properties via Mo addition in Al-Mn-Mg 3004 alloy, J. Alloys Compd. 694 (2017) 354–365, https://doi.org/10.1016/j.jallcom.2016.10.005.

[40] B. Lin, W. Zhang, X. Zheng, Y. Zhao, Z. Lou, W. Zhang, Developing high performance mechanical properties at elevated temperature in squeeze cast Al-Cu-Mn-Fe-Ni alloys, Mater. Charact. 150 (2019) 128–137, https://doi.org/10.1016/j.matchar.2019.01.022.

[41] A. Shyam, S. Roy, D. Shin, J.D. Poplawsky, L.F. Allard, Y. Yamamoto, J.R. Morris, B. Mazumder, J.C. Idrobo, A. Rodriguez, T.R. Watkins, J.A. Haynes, Elevated temperature microstructural stability in cast AlCuMnZr alloys through solute segregation, Mater. Sci. Eng. A 765 (2019), https://doi.org/10.1016/j.msea.2019.138279.

[42] J. Chen, H. Liao, Y. Wu, H. Li, Contributions to high temperature strengthening from three types of heat-resistant phases formed during solidification, solution treatment and ageing treatment of Al-Cu-Mn-Ni alloys respectively, Mater. Sci. Eng. A 772 (2020), https://doi.org/10.1016/j.msea.2019.138819.

[43] G. Li, H. Liao, J. Zheng, M. Yang, L. Qian, M. Shi, L. Lu, Synergistic effect of joint addition of Sb+Mn on high temperature strengthening in Al–4Cu heat-resistant alloy, Mater. Sci. Eng. A 851 (2022), https://doi.org/10.1016/j.msea.2022.143623.

[44] G. Li, H. Liao, J. Zheng, H. Chen, L.Z. Lu, L. Yang, H. Guo, Micro-alloying effects of Mn and Zr on the evolution of ageing precipitates and high temperature strength of Al-11.5Si–4Cu alloy after a long-time heat exposure, Mater. Sci. Eng.: A 828 (2021), https://doi.org/10.1016/j.msea.2021.142121.

[45] G. Li, X. Pan, H. Liao, J. Zheng, M. Yang, L. Qian, L. Lu, Sn-induced phase transformation mechanism from θ' to θ in Al-4Cu alloy and its influence on high temperature strength, Trans. Nonferrous Met. Soc. China (English Edition) 33 (2023) 2559–2573, https://doi.org/10.1016/S1003-6326(23)66281-8.

[46] E.R. Wang, X.D. Hui, G.L. Chen, Eutectic Al-Si-Cu-Fe-Mn alloys with enhanced mechanical properties at room and elevated temperature, Mater. Des. 32 (2011) 4333–4340, https://doi.org/10.1016/j.matdes.2011.04.005.

[47] L. Han, Y. Sui, Q. Wang, K. Wang, Y. Jiang, Effects of Nd on microstructure and mechanical properties of cast Al-Si-Cu-Ni-Mg piston alloys, J. Alloys Compd. 695 (2017) 1566–1572, https://doi.org/10.1016/j.jallcom.2016.10.300.

[48] A.R. Farkoosh, X. Grant Chen, M. Pekguleryuz, Dispersoid strengthening of a high temperature Al-Si-Cu-Mg alloy via Mo addition, Mater. Sci. Eng.: A 620 (2015) 181–189, https://doi.org/10.1016/j.msea.2014.10.004.

[49] H.Q. Liu, J.C. Pang, M. Wang, S.X. Li, Z.F. Zhang, Effect of temperature on the mechanical properties of Al–Si–Cu–Mg–Ni–Ce alloy, Mater. Sci. Eng. A 824 (2021), https://doi.org/10.1016/j.msea.2021.141762.

[50] J. Huang, D. Ando, Y. Sutou, Heat-resistant aluminum alloy design using explainable machine learning, Mater. Des. 243 (2024), https://doi.org/10.1016/j.matdes.2024.113057.

[51] X. Na, L. Wenqing, Z. Liu, T. Muthuramalingam, Effect of scandium in Al–Sc and Al–Sc–Zr alloys under precipitation strengthening mechanism at 350 °C aging, Met. Mater. Int. 27 (2021) 5145–5153, https://doi.org/10.1007/s12540-020-00844-0.

[52] D. Turnbull, B. Vonnegut, Nucleation catalysis, Ind. Eng. Chem. 44 (1952) 1292–1298.

[53] Y. Liu, L. Luo, C. Han, L. Ou, J. Wang, C. Liu, Effect of Fe, Si and cooling rate on the formation of Fe- and Mn-rich intermetallics in Al-5Mg-0.8Mn alloy, J Mater. Sci. Technol. 32 (2016) 305–312, https://doi.org/10.1016/j.jmst.2015.10.010.

[54] A. Mohammadi, N.A. Enikeev, M.Y. Murashkin, M. Arita, K. Edalati, Examination of inverse Hall-Petch relation in nanostructured aluminum alloys by ultra-severe plastic deformation, J. Mater. Sci. Technol. 91 (2021) 78–89, https://doi.org/10.1016/j.jmst.2021.01.096.

[55] V.C. Nardone, K.M. Prewo, On the strength of discontinuous silicon carbide reinforced aluminum composites, Scr. Metall. 20 (1986) 43–48, https://doi.org/10.1016/0036-9748(86)90210-3.

[56] E.O. Hall, The deformation and ageing of mild steel: III discussion of results, Proc. Phys. Soc. B 64 (1951) 747–753, https://doi.org/10.1088/0370-1301/64/9/303.

[57] N.J. Petch, The cleavage strength of polycrystals, J. Iron Steel Inst. 174 (1953) 25–28.

[58] K. Dou, E. Lordan, Y. Zhang, A. Jacot, Z. Fan, A novel approach to optimize mechanical properties for aluminium alloy in high pressure die casting (HPDC) process combining experiment and modelling, J. Mater. Process Technol. 296 (2021), https://doi.org/10.1016/j.jmatprotec.2021.117193.

[59] Y. Zhang, E. Lordan, K. Dou, S. Wang, Z. Fan, Influence of porosity characteristics on the variability in mechanical properties of high pressure die casting (HPDC) AlSi7MgMn alloys, J. Manuf. Process 56 (2020) 500–509, https://doi.org/10.1016/j.jmapro.2020.04.071.

[60] N. Hansen, The effect of grain size and strain on the tensile flow stress of aluminium at room temperature, Acta Metall. 25 (1976) 863–869, https://doi.org/10.1016/0001-6160(77)90171-7.

[61] T. Uesugi, K. Higashi, First-principles studies on lattice constants and local lattice distortions in solid solution aluminum alloys, Comput. Mater. Sci. 67 (2013) 1–10, https://doi.org/10.1016/j.commatsci.2012.08.037.

[62] J.P. Hirth, J. Lothe, Theory of Dislocations, second, Wiley, New York, 1982.

[63] O.R. Myhr, Ø. Grong, S.J. Andersen, Modelling of the age hardening behaviour of Al-Mg-Si alloys, Acta Mater. 49 (2001) 65–75, https://doi.org/10.1016/S1359-6454(00)00301-3.

[64] G. Du, J. Deng, Y. Wang, D. Yan, L. Rong, Precipitation of (Al,Si)3Sc in an Al-Sc-Si alloy, Scr. Mater. 61 (2009) 532–535, https://doi.org/10.1016/j.scriptamat.2009.05.014.

[65] O.D. Sherby, R.A. Anderson, J.E. Dorn, Effect of alloying elements on the elevated temperature plastic properties of alpha solid solutions of aluminum, JOM 3 (1951) 643–652, https://doi.org/10.1007/BF03397360.

[66] S. Zhang, H. Du, Z. Yao, Z. Liu, Y. Zhu, L. Shuai, T. Huang, X. Huang, X. Tao, D. P. Mondal, T. Akopyan, N. Belov, Superior high temperature creep resistance of a cast Al–Mg–Ca-Sc alloy with multi-scale hierarchical microstructures, Mater. Sci. Eng. A 850 (2022), https://doi.org/10.1016/j.msea.2022.143533.

[67] D. Odoh, Y. Mahmoodkhani, M. Wells, Effect of alloy composition on hot deformation behavior of some Al-Mg-Si alloys, Vacuum 149 (2018) 248–255, https://doi.org/10.1016/j.vacuum.2017.12.037.

[68] L. Wang, B. Ye, W. Huang, W. Ding, Theoretical model of yield strength for eutectic colony microstructure materials, Scr. Mater. 231 (2023), https://doi.org/10.1016/j.scriptamat.2023.115443.